The key element of such an image processing and computational system is the extraction of the vascular luminal surface from medical image data; the term *segmentation* is traditionally used for this procedure. The subsequent steps—volume mesh generation and flow modeling—are traditional and well-established procedures in CFD. A few approaches to segmentation are known from the literature. The initial stage in most of them is the performance of separate luminal segmentation for each 2D image or data section. At the next stage, once the series of lumen contours is obtained, the luminal surface is reconstructed by using splines (16), contour tiling (17) or other similar methods. The main disadvantage of this rather sophisticated approach is that it involves a great deal of manual, time-consuming work, especially in complex geometries with branching vessels (16). No integrated, commercially available software packages seem to offer such segmentation methods. In most cases, researchers use codes developed in-house or combinations of commercial codes, libraries, and in-house developments (8, 18, 19). Computer-aided drafting (CAD) systems, which are fairly difficult to learn and operate, are often involved (18, 19). Thus, it is not easy for clinicians to implement such methods and use them in their daily practice if they do not have substantial knowledge of computer graphics, computational mathematics, and related fields.

It is generally obvious that a direct 3D segmentation technique (without resorting to 2D contours) allows a higher degree of automation (20, 21). An interesting and time-efficient virtual balloon method (22) has been proposed; in it, a spherical balloon with a triangulated surface is inserted inside the lumen and then inflated to assume the shape of the lumen. At present, implementation of the technique requires its programming from scratch. It also remains to be seen how it would perform for really complex geometries; the example of a branching vessel given in reference 22 is fairly simple.

We sought to determine how 3D imaging data collected in DICOM format can be used to create numerical grids for computer simulations of blood flow in a relatively simple way that non-CFD specialists could perform after minimum training. To achieve this goal, we used well-established, commercially available software packages, particularly Advanced Visual Systems/Express software, to extract luminal vessel surfaces; this was done with the easy and automatic procedure of isosurfacing at an operator-specified gray-scale value. This approach also belongs to the direct 3D segmentation methods, which immediately result in a triangulated 3D luminal vascular surface.

Methods

The flowchart of patient-specific computational grid reconstruction and blood flow numerical simulation in Figure 1 indicates the main tools (numbered 1–6) of the procedure and the respective output formats (a–f). The whole process consists of five logical steps (I–V). In step I, primary medical images in DICOM format are obtained. In step II, they are transformed into a format suitable for the software that will be extracting

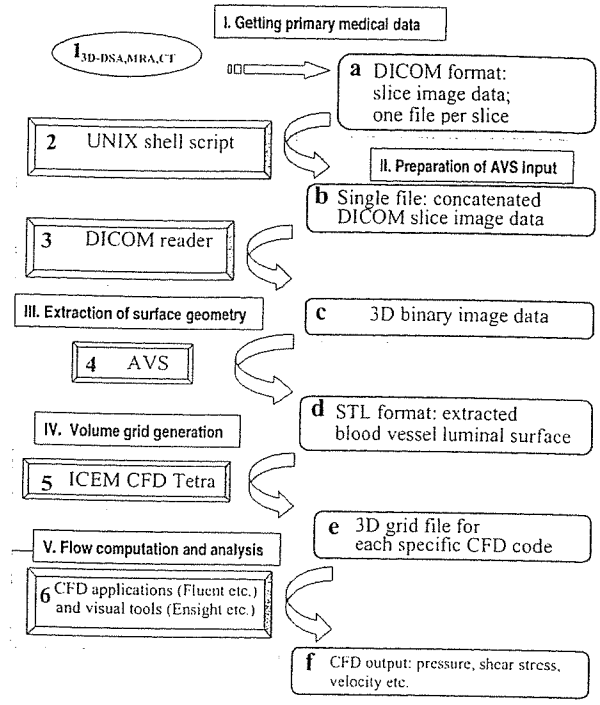

FIG 1. Flowchart of patient-specific segmentation, volume grid generation and blood flow analysis shows software tools (1–6) and output formats (a–f). I–V denote major stages of the procedure.

the luminal surface of the blood vessels of interest in step III. In step IV, the surface data are then imported by a grid generator, which creates a volume grid. The resulting grid model is used at step V for the numerical simulation of blood flow.

Rotational Digital Subtraction Angiography:

We obtained 3D datasets (Advantx UNV; GE Medical Systems, Milwaukee, WI) from rotational series consisting of two rotations. The first rotation provided the subtraction mask. The C-arm was rotated 200° in 5 seconds at the exposure rate of 8.8 frames per second. A total of 44 images with a matrix size of 512 × 512 pixels were acquired. The second rotation was performed simultaneously with the administration of contrast material. All 88 images were immediately transferred via our network to a workstation (Advantage Unix; GE Medical Systems) for volume analysis. A 3D reconstruction algorithm based on the algebraic reconstruction technique was used to digitally produce 3D digital subtraction angiography (DSA) images (Fig 2A and B) on the workstation within 8 minutes. Algorithms were maximum intensity projection (MIP) and surface-shaded display (SSD) at an isosurface with a mean threshold value of 1100 H.

The image displayed on the monitor was subjected to reformatting into transverse regularly spaced sections (Fig 2C). The batch function of the volume analysis allowed us to set up this set of sections rapidly. It was possible to preview the set as an animated sequence (movie loop) and save it on the image disk as sections in secondary DICOM format (Fig 2D). At the end of this stage, a separate data file for each section was generated. The file contained image data and other relevant information, such as the image size and patient's name.

Larger numbers of sections and decreased spaces between them improved the final mesh quality. In our experience, the number of sections for 3D DSA should be in the range of 300–700 sections, with a 0.1–0.2-mm distance between the

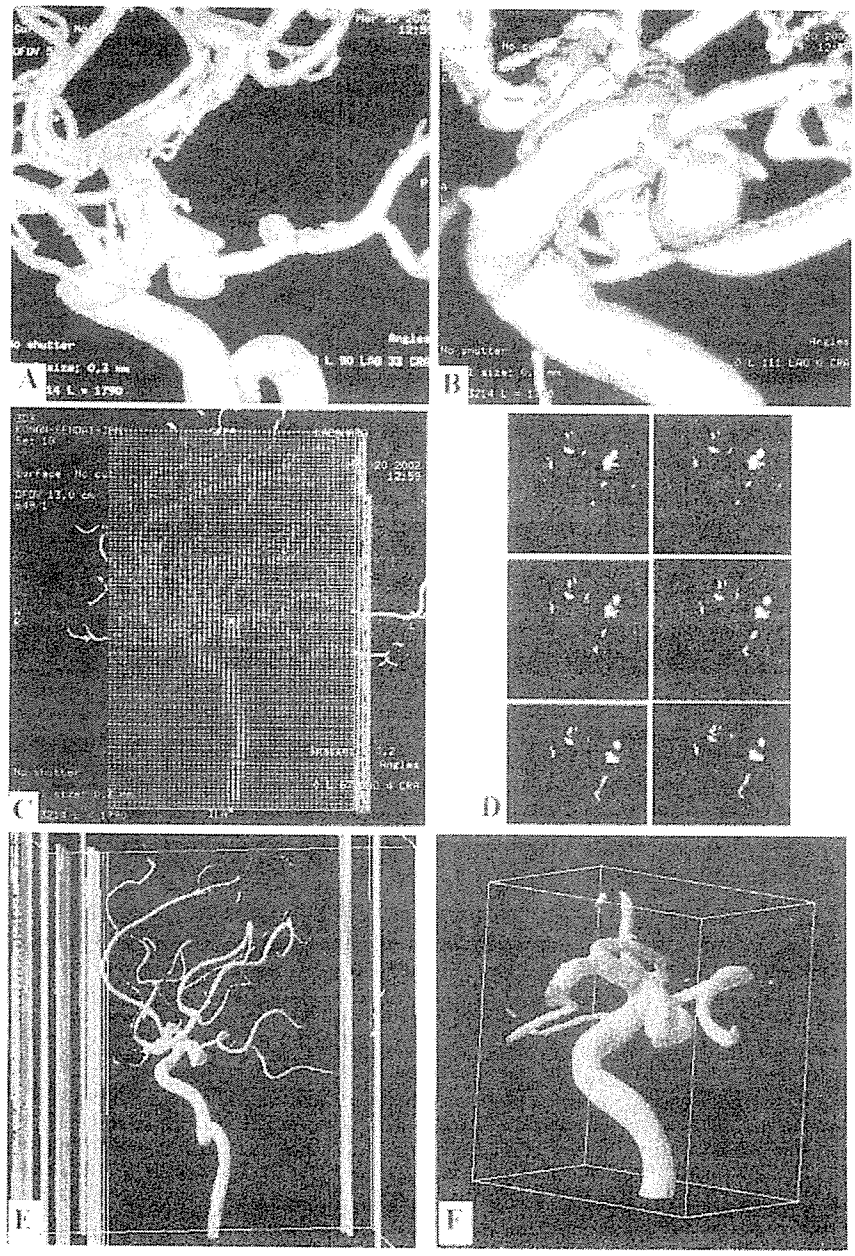

FIG 2. Data transformation from an angiographic image into a computational grid model.

A and *B*, 3D DSA images (different views) of a posterior communicating artery aneurysm.

C, Typical setup for reformatting of the angiographic image into 585 secondary DICOM sections in a 13-cm displayed field of view.

D, Sequential secondary DICOM sections. The respective files are concatenated before processing with DICOM reader (X) MedCon.

E, 3D gray-scale raster image produced by (X) MedCon and imported by AVS/Express. Columns are patient data and image parameters still present in the file.

F, Result of image manipulations with AVS/Express. ROI is cut out and the luminal vascular surface is identified with a gray-scale isosurface value of 1500. This ROI includes the aneurysm and its small branching vessel. (Figure continues.)

sections and a 0.3–1-mm section thickness (equal to 1 voxel). Section sets of less than 300 images were not promising in terms of final computational mesh quality.

MR Angiography

3D time-of-flight (TOF) MR angiography (MRA) was performed by using a 1.5-T MR imaging system (Signa Horizon; GE Medical Systems). A standard head coil was used for imaging of the head (Fig 3A). 3D TOF MRA was performed by using the following imaging parameters: TR/TE, 30/3.2; flip angle, 20°; section thickness, 0.8 mm; slab thickness, 64 mm; matrix, 256 × 256; and field of view, 16 cm.

CT Angiography

CT angiography (CTA) was done by using a helical CT scanner (LightSpeed Plus-U; GE Medical Systems) with multidetector-row capability (where one scan equaled eight sections). The data presented in Figure 3 were obtained by using a section thickness of 1 mm with a 0.63-mm interval between the sections and a table speed of 8.75 mm/s (140 kV, 180 mAs). Zero-degree table and gantry tilt were used. Sections in DICOM format were acquired with a 512 × 512 matrix. Scanning was started at the C1 level and continued cranially parallel to orbitomeatal line to the skull vertex during the intravenous injection of contrast material at a rate of 3 mL/s.

The digital images and the respective files obtained so far could not be directly used for grid generation. The luminal surface of blood vessels was extracted from them in the format suitable for import by grid generators. This was done, for instance, by using the Advanced Visual Systems/Express (AVS/Express Visualization Edition, version 5.1). Step II and tools 2 and 3 of our procedure (Fig 1) were needed to convert our files into a proper format for AVS/Express input.

Merging of Section Files and DICOM Reader Software

First (Fig 1, tool 2), all DICOM files were combined into a single one, a standard operation for any computer operating

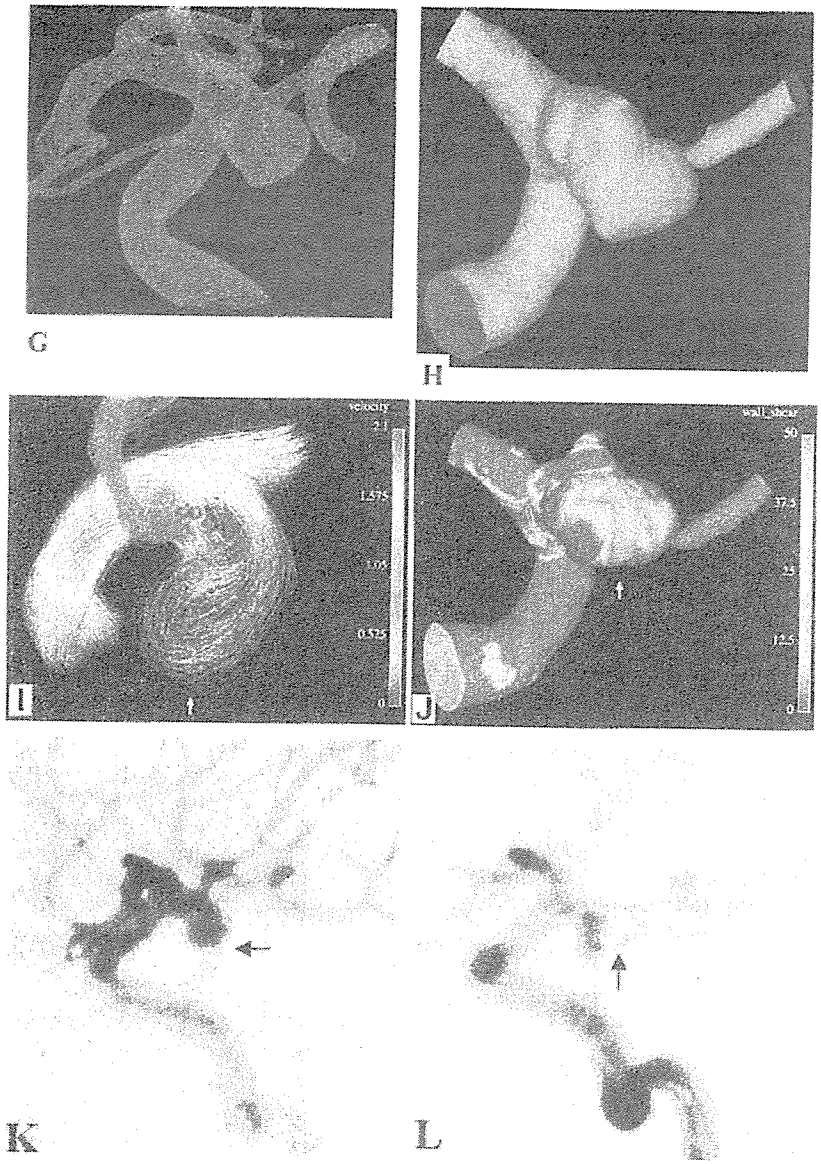

FIG 2. Continued.

G, AVS/Express STL file containing the surface mesh is imported by using the ICEM CFD Mesh Editor and Tetra grid generator. These tools allow us to further remove unnecessary parts, manually repair and smooth the surface mesh, close inflow and outflow boundaries, and generate the volume grid.

H, Final computational tetrahedral grid model for blood flow simulation with Fluent or another suitable software.

I, Typical instant streamlines colored by velocity (in m/s) show that the entering bloodstream hits the aneurysm wall at the angiographically determined rupture area (*arrow*).

J, Typical instant wall shear-stress distribution (Pa) shows a local shear-stress maximum where the aneurysm ruptured (*arrow*).

K, Arterial-phase 2D DSA image shows escape of a linear stream of contrast agent into the subarachnoid space (*arrow*).

L, Arterial-phase 2D DSA image obtained during endovascular intervention shows escape of the coils through the aneurysm rupture (*arrow*).

system (eg, Unix, Windows, Mac OS). In the present work, this was done on a Unix computer with the concatenate command. With Microsoft Windows, the copy command allowed us to perform such file merging.

Second, (Fig 1, tool 3), the resulting single file was imported by using the X-windows medical image conversion utility (X) MedCon (version 0.5.10; Erick Nolf, Ghent University Hospital, Ghent, Belgium). The conversion utility always used original image dimensions and pixel values. This DICOM reader could output files in raw binary or ASCII formats. The binary output format included binary image data with all other information (eg, image size, patient's name) contained in the original section image files. This additional information was to be cut later by using AVS/ Express. The resulting file at this stage contained a 3D raster gray-scale image (Fig 2E). (More details can be found at *http://xmedcon.sourceforge.net.*)

AVS/Express Visual Development Tool

The main role of the AVS/Express visual development tool (AVS, Waltham, MA) (Fig 1) was to define the region of interest (ROI) and to extract the luminal vascular surface from the 3D raster gray-scale image obtained at the previous stage (Fig 2). Detailed information about AVS commands may be obtained at *www.avs.com*.

Using the AVS isosurface command, we could extract the luminal vascular surface, triangulating it and writing into a file in stereolithography (STL) format. It used voxel intensities ranging from 0 to 4000. The procedure was fully automatic and based on picking up the data corresponding to some specified fixed value and connecting the respective points, thus forming surface triangles. In our experience, the specific gray-scale isosurface value corresponding to the luminal vessel surface could be determined by trial and error, aiming at the best appearance of the surface, in a range from 1100 to 1800 for 3D DSA data and in a range of 200–400 for MRA and CTA data. The STL format could be used as geometry input format in most modern commercial grid generators (Figs 2F, 3B, and C).

Measurements of maximum aneurysmal diameters, aneurysmal neck diameters, diameters of parent arteries, and other dimensions were performed on the luminal vascular surfaces in the 3D DSA images and their respective reconstructed meshes. The comparable measurements were statistically analyzed by using multiple regression analysis (StatView, version 5.0.1; SAS Institute, Cary, NC). The error probability values ($P < .0001$) and the estimated standard error (SE = 0.007) were calculated.

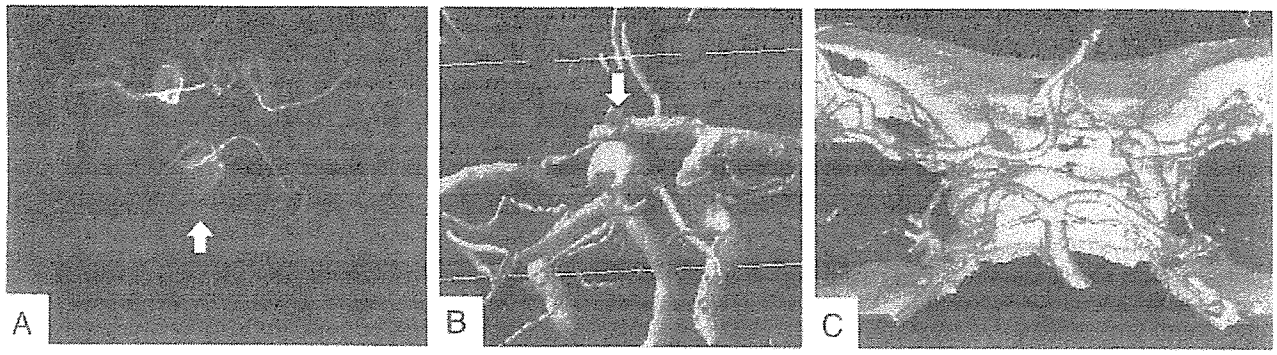

FIG 3. Examples of four vessels reconstructed from MRA image and CTA data.
A, MRA data of four vessels with basilar top aneurysm (arrow).
B, Surface grid reconstruction of MRA image data. Note the inferior quality of this grid, as compared with that obtained from 3D DSA and multiple defects in the vessel walls.
C, Surface grid reconstruction (STL file) from CTA of four vessels of a normal circle of Willis. Note the reconstructed skull base requiring manual removal during mesh generation.

Grid Generator

The next stage (Fig 1, stage IV) was volume grid generation. The grid generation software (ICEM CFD version 4.1; ICEM CFD Engineering) was used to divide our model into tetrahedral cells. (Tetrahedral grids are widely used in CFD for computational models of complex shape.) The Mesh Editor and Tetra tools allowed us to cut additional unnecessary parts not related to our ROI to close the computational domain to define inlets, outlets, and wall boundaries (Fig 2G and H). Interactive modifications of the individual grid node coordinates could be done as well to eliminate unneeded small branches and false vessel connections. Finally, mesh smoothing further improved grid quality. The grid generator also allowed us to construct a triangular, prismatic, layered mesh representing vascular walls of finite thickness. This was needed for coupled flow-dynamic and elastodynamic simulations that took into account the deformations, stresses, and displacements of the vessel walls (Fig 4). (Further details can be found at *www.icemcfd.com.*)

The number of grid nodes or tetrahedrons was chosen as a reasonable compromise between better accuracy and shorter computational time of subsequent simulations. In the ICEM CFD grid generator, a nondimensional parameter Tetra determined the size of tetrahedral mesh units to be generated and, hence, the number of grid nodes, the mesh resolution, and the accuracy of the subsequent calculations. Test computations were performed for the same model with different Tetra values: 1.0, 0.5, and 0.25. It was found that the Tetra value 0.5 was small enough to get a reasonably converged solution (ie, further reduction of the parameter did not lead to considerable changes in the solution) within acceptable computational time. The numbers of nodes and tetrahedrons in the grids used to compute the cases presented in Figures 2 and 5 were within the ranges 26,000–48,000 and 170,000–285,000, respectively. The prismatic-tetrahedral grids in Figure 4 contain 7049 (case I) and 17,060 (case II) nodes.

Computational grids obtained from stages I–IV (Fig 1) could be applied to numerical simulations of blood flow in the respective geometry by using CFD software (Fidap; Fluent Inc., Lebanon, N.H.).

Flow Modeling

The unsteady 3D incompressible Navier-Stokes equations are widely used for blood flow simulations. Blood is usually considered a Newtonian fluid; this is a fairly good approximation for large-bore vessels. Our simulations were performed with the following material constants: blood density, 1060 kg/m^3; and blood dynamic viscosity, 0.004 Poiseuille.

To achieve truly patient-specific modeling, the boundary condition at the inflow boundary was based on the pulsatile periodic flow rate obtained during sonography of intracranial vessels. Because the governing equations and boundary conditions included only the pressure gradient, the simulation produced relative pressure values to be considered with respect to a basal pressure.

The unsteady flows in aneurysms were computed for an interval of 3 seconds (over three cardiac cycles). The results corresponding to the last, third cycle were considered independent of the initial conditions and used for flow analysis. We performed several computations for the same model with different time steps: 0.1 second (30 steps), 0.025 second (120 steps), and 0.01 second (300 steps). As long as the grid-converged solution was obtained (ie, the grid was fine enough), the time step values did not dramatically influence the results at a certain instant of the cardiac cycle (eg, at the systolic peak). The time step of 0.025 second seemed to provide a reasonable compromise in terms of accuracy and computational time and for plotting and statistical analysis.

As to the walls of the vessels, two main possibilities exist. The first and simplest approach was to consider them as rigid structures. The second was to account for their movement and deformation. In the latter, an elastic model was chosen, with its parameters to be determined.

Rigid Vessels

Under this assumption, any CFD code with incompressible fluid-modeling capabilities can be used. We applied Fluent software (version 6.0.12) (Fluent Inc., Lebanon, NH) to compute physiologic pulsating flows. In the code, the governing equations written in strong conservative form for mass and momentum were discretized with a finite-volume method. We chose the SIMPLE method to solve the discretized equations. To improve the convergence speed, relaxation factors were applied to velocity and pressure modifications. (Detailed information about the code is available at *www.fluent.com.*)

On the rigid vessel walls, the nonslip and nonpenetration conditions were applied (ie, all velocity components at the vessel walls were set to zero). For the outlet, the Fluent outflow boundary condition was used. The typical computational time on the grids just mentioned was approximately 8–12 hours on a single processor (Origin 2000; Silicon Graphics Inc).

Deformable Vessels

This model required a fluid-structure interaction approach accounting for both instantaneous fluid forces acting on the walls of vessels and for effects of the walls' motion on the fluid dynamic field. The number of software packages that included fluid-structure interaction capabilities was relatively limited.

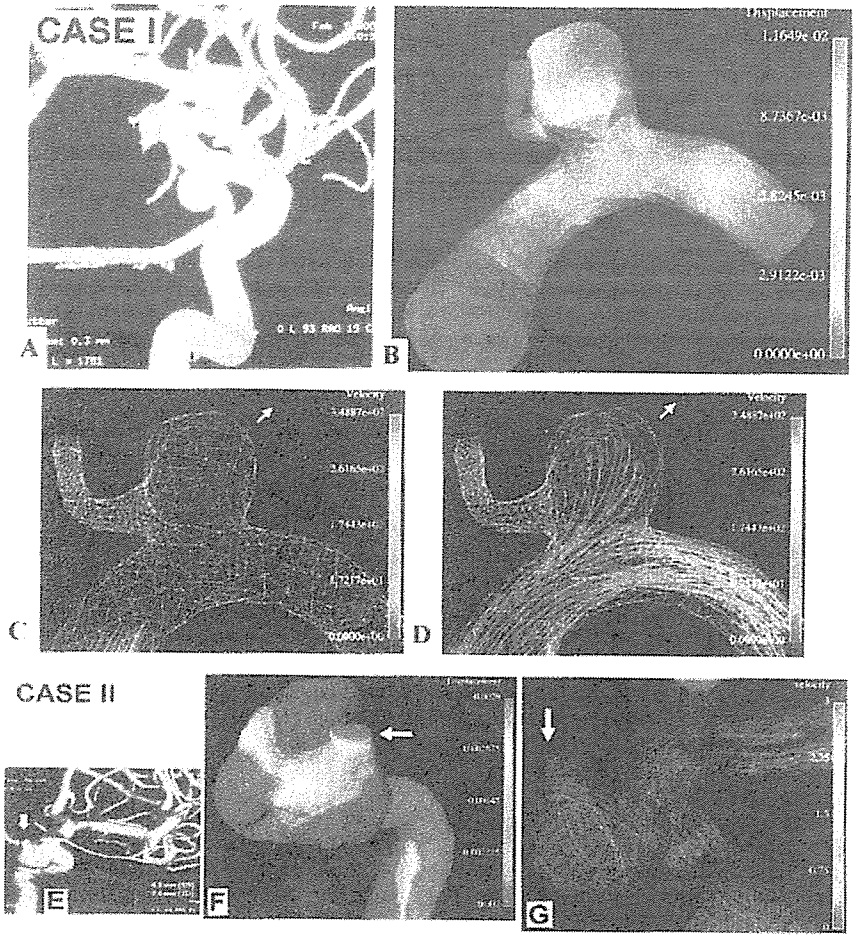

FIG 4. Computations for grid models with moving walls. Case I: *A*, 3D DSA image of a nonruptured internal carotid–posterior communicating aneurysm. *B*, Displacement (in mm) of the aneurysm wall at the systolic peak. *Red* is maximal displacement. *C* and *D*, Movie frames illustrate deformation of the aneurysm from early systole (*C*) to midsystolic peak (*D*). *Arrow* indicates the direction of movement (and possible future growth). Bloodstream enters the aneurysm, hits its wall, decelerates (note change in color; velocity in cm/s), and exerts pressure resulting in maximal displacement. Case II: *E*, 3D DSA image of a nonruptured carotid cave aneurysm. *F*, Displacement of the aneurysm wall at the systolic peak. *Red* is maximal displacement at the nonruptured aneurysmal bleb (*arrow*). *G*, Typical instant streamlines show that the entering bloodstream hits the aneurysm wall at the angiographically determined bleb (*arrow*), exerting pressure that results in maximal displacement.

Fidap (Fluent Inc., Lebanon, NH) code was used to carry out the simulations presented in Figure 4.

In this code, an Arbitrary Lagrangian Eulerian (ALE) algorithm was used. This sought, at each time increment, the convergence of three blocks of equations describing blood dynamics, stresses in vessels' walls, and mesh movements (23). The only Fidap option for vascular walls was a linear elastic homogeneous approximation. The following elastic material constants were used: Young modulus of 2.7 Mpa and Poisson coefficient of 0.45 (18). The cases in Figure 4 took more than 4 days to compute on a single processor (Origin 2000; Silicon Graphics Inc). (A description of Fidap can be found at *www.fluent.com*.)

Flow Visualization

Fluent, Fidap, and other CFD software packages have their own visualization tools that are sufficient in many cases. However, specialized postprocessing software might offer additional useful options. For instance, we used EnSight (version 7.3.0; Computational Engineering International Inc., Apex, NC), which was general-purpose postprocessing software used in engineering and research and available for all major computer platforms. This was used to create computer animations (movies) of unsteady blood flow through aneurysms based on Fluent and Fidap results (Fig 5). (Details can be found at *www.ensight.com*.)

Results

Figure 2 shows data from a patient with ruptured internal carotid–posterior communicating artery aneurysm and illustrates the whole procedure of computational analysis from 3D DSA to CFD results. The ruptured area was depicted by using angiography (Fig 2K and L). Comparison with the simulation results allowed us to conclude that it corresponded to the area facing the bloodstream entering the aneurysm. The aneurysm wall served as an obstacle decelerating the entering stream (diminishing its velocity) and deflecting it along the wall. This was accompanied by a persisting local fluid-induced wall shear-stress maximum in the area hit by the stream; this might have been one of the reasons for aneurysm rupture.

Figure 3 illustrates surface grid extractions from MRA of the circle of Willis and CTA. One image shows multiple defects in the wall of the basilar artery aneurysm that made surface mesh repair and volume grid generation more time- and labor-consuming than they would have been with "clean" 3D DSA images. Nevertheless, there were no fundamental difficulties, and surface grid reconstruction for sparsely sampled MRA-based objects was attainable with the proposed approach. CTA showed promising mesh quality that may be useful for studying flow dynamics of the intracranial vessels. However, manual removal of the reconstructed skull base bone was necessary.

Figure 5 illustrates another attempt at computational diagnosis of the rupture area of MCA aneurysms, with subsequent surgical validation. Similar to

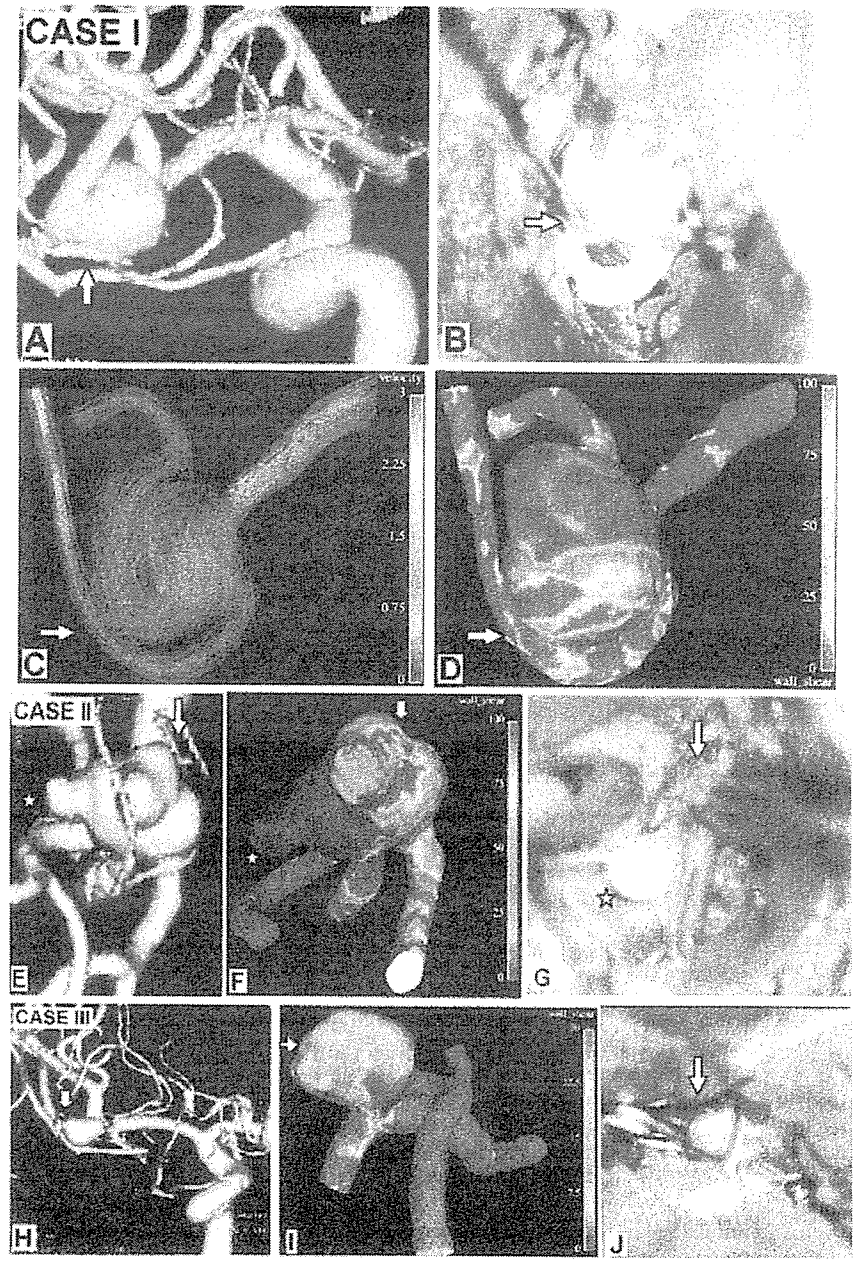

FIG 5. Computational results for grid models with rigid walls compared with operative photos and 3D DSA images. Case I: *A*, 3D DSA shows a ruptured middle cerebral artery (MCA) bifurcation aneurysm. *B*, Operative photo shows the aneurysm and a curved branch coming from it, the lower trunk of the MCA. Note a surgical instrument pointing to the ruptured zone on the aneurysm wall (*arrow*) under the genu of the lower trunk of the MCA. *C*, This zone faces the blood stream entering the aneurysm (*arrow*, *velocity* in *m/s*). *D*, Wall exposed to high shear stress (*arrow*, units of Pa). Case II: *E*, 3D DSA of a ruptured MCA bifurcation aneurysm with multiple blebs. *F*, Typical instant wall-shear-stress distribution (Pa) shows a local shear-stress maximum where the aneurysm ruptured (*arrow* in *F*). Largest bleb (*star*) in the low-shear-stress area of the aneurysm wall. *G*, At surgery, this was not ruptured and had an intact wall. Dome blebs in the high shear stress area (*arrow*) in front of the coming bloodstream were the ruptured ones and were tentatively clipped (*arrow*). Case III: *H*, 3D DSA image of a small, ruptured MCA bifurcation aneurysm. *I*, Typical instant wall-shear-stress distribution shows a local shear-stress maximum where the aneurysm ruptured (*arrow*). 3D orientations of the aneurysm are similar in *I* and *J*, an operative photo showing the aneurysm in the sylvian fissure after proximal clip placement of the MCA and a thin-walled, ruptured area (*arrow*) where the aneurysm had maximum local shear stress.

a previous case (Fig 2), the ruptured area corresponded to the area where the entering blood stream first hit the wall (at an angle). Again, high wall-shear stress was seen in this area; this might have been the reason for rupture at this location.

Case I in Figure 4 (nonruptured internal carotid–posterior communicating artery aneurysm) represented successful 3D modeling that accounted for vascular movement and deformation by using Fidap. In correspondence with the findings illustrated in Figures 2 and 5, this figure identified the maximum area of displacement as the area hit by the blood jet entering the aneurysm. The aneurysm was likely to grow in this direction. It was also a primary suspect for the location of possible rupture or bleb formation, as shown in case II in the same figure (nonruptured carotid cave aneurysm). These findings confirmed that the maximum area of wall displacement is located at the angiographically determined bleb in the aneurysmal inflow zone.

Discussion

The method for anatomic reconstruction of cerebral vessels in the form of computational replicas should work for a broad spectrum of medical imaging techniques, the availability of which varies from one medical center to another. Replicas were obtained from all currently available modalities of cerebral angiography, such as noninvasive screening MRA and CTA, which can sometimes replace 3D DSA in diagnosing intracranial aneurysms (24, 25) and also the invasive, highest-quality 3D DSA. Therefore, our approach was general: It worked with any 3D image

data in DICOM format as the source of original information, and it could produce grid output for virtually any commercial CFD software.

Segmentation (Surface-Extraction) Techniques

In our approach, the entire set of cross-sectional images (sections) obtained from angiographic machines was immediately fused into a single 3D DICOM image by means of simple file merging. The DICOM reader then converted the DICOM file into a binary format suitable for use with image processing and visualization software, such as AVS/Express. Therefore, in AVS/Express we directly manipulated the original source output of the angiography machines without any modifications and used it to extract the luminal surface. This approach substantially contributed to the simplicity and stability of operations and minimized possible errors of image interpolation.

Direct 3D segmentation in AVS/Express by means of isosurfacing is simple and fully automatic and requires minimal effort; this is in contrast to the sophisticated image-segmentation methods based on 2D (section-by-section) segmentation with the subsequent reconstruction of 3D luminal surface geometry (26–30). These methods usually require a computer graphics or computational mathematics specialist to accomplish them. Isosurfacing is conceptually close to the virtual balloon inflation technique (22), which is also based on direct 3D segmentation.

The average time of image segmentation from DSAs or MRAs into luminal surface meshes (STL files) is about 30 minutes. The resulting surface meshes from densely sampled high-spatial-resolution data (eg, DSA images) are of high quality. They need no or only minor manipulations in the mesh generator before volume mesh generation (which is an automatic procedure). Sparsely sampled objects (eg, MRA images) have lower spatial resolution and therefore result in a lower-quality surface mesh. These need more effort from the examiner to remove image artifacts and to repair and smooth the surface mesh before tetrahedral mesh generation (26). Future advances in angiographic technology to further improve DSA image quality will certainly simplify and improve the accuracy of luminal surface segmentation by means of isosurfacing.

3D images are manually optimized to define the vascular luminal surface before volume grid generation. Therefore, correction for the penumbra effect (unsharpness of edge determination due to diminished contrast resolution as the luminal vascular boundary is approached) is operator-dependent with this method.

Our experience with segmentation by means of isosurfacing in AVS shows that obviously false communications (eg, between small arteries and an aneurysm) may arise when we use an isosurface value that otherwise seems optimal for the most accurate representation of the luminal surface. Although such false connections can be eliminated by increasing the isosurface value, we recommend keeping this value and removing it later in the ICEM CFD grid generator and mesh editor.

The choice of ROI primarily depends on the examining physician and on what he or she wants to achieve from the whole procedure. At best, we know only the mean flow parameters in vessels as a function of time. This is why we should set our inflow and outflow boundaries "far enough" so that our insufficient knowledge does not influence the flow in the aneurysm under study. The uncertainties in the inflow-outflow parameters are at least of the same significance as that of errors produced by the location of inflow-outflow boundaries. However, physicians using CFD should have some knowledge of incompressible fluid dynamics, or they should solicit help from a fluid dynamics specialist to learn about the possible strong fluid dynamic effects proximal and distal to the aneurysm; such effects are due to factors such as severe arterial curvature, which may cause large secondary flows. The inflow boundary should be set within unidirectional fluid flow without any vortices or secondary flows.

Special attention should be paid to cutting out ROI and downsizing the image. Minimization of the ROI is important to decrease computational time (for both grid generation and computation itself), making it possible to finish the patient-specific image processing and computational procedure in 1 day. In our experience, the average time needed for calculation of the ROI limited to the aneurysm zone (about 5 hours) was shorter than that needed to calculate the whole parent artery with the aneurysm (about 2 days), when the results inside and near the aneurysm are confirmed to be the same for both ROIs. Nevertheless, these considerations about the possible influence of inflow-outflow boundaries on the results should be always kept in mind.

CFD by Physicians

The knowledge and skills needed to conduct CFD studies—including some elementary background in incompressible fluid mechanics and computational methods—are comparable to those needed to conduct, understand, and interpret radiologic studies (eg, MR, CT, SPECT, and PET images). Therefore, physicians themselves will undoubtedly perform CFD analysis in the future. In the mean time, because such CFD studies are still a relative novelty under development, they should be initially conducted under the supervision of a fluid dynamicist to establish a reliable technique and to correlate the results with radiologic or operative information. Now we rely on a set of commercially available software packages that might soon be replaced by a single, integrated technician-operable software package. Physicians should not straightforwardly rely on the first results that they receive from CFD computations to detect the possible location of an aneurysm rupture. A comparative, blinded study should be first conducted in any institution looking for applications of CFD before the whole numerical procedure is proved correct and

time-efficient. Only after that can this code be used more widely in clinical work.

CFD as a Useful Clinical Tool

Applications of CFD as an assisting tool for studying patient-specific hemodynamics are becoming more practical. Several clinical applications of CFD in cerebral aneurysms of real patients have been described (31, 32, 33). Detection of the rupture area of intracranial aneurysms before surgery is important for every neurosurgeon. Although somewhat simplistic modeling that assumes rigid vessel walls may be promising for this purpose in some cases (such as those shown in Figure 5) because of the relatively short computational time. In these cases, the whole computational analysis lasted an average of approximately 8 hours, which makes it possible to treat patients the same day as an acute hemorrhage; this method provides CFD results, if needed, before surgery.

For the cases presented in Figures 2 and 5, the ruptured area of the aneurysms geographically corresponded to the area in which the bloodstream entering the aneurysm hit its wall. This area also corresponded to relatively high pressure- and fluid-induced wall shear stress in the aneurysms. This finding would not have been possible without angiographic or operative confirmation. In general, when a blood jet impinges on an aneurysm wall, there is a stagnation point at which pressure is maximal but wall shear stress is zero. Around this localized high-pressure spot is a large area of high wall shear stress caused by the bloodstream turning along the aneurysmal wall; this is where rupture happens, as seen in our cases.

In realistic acrylic aneurysmal models, Tateshima et al (4) found that the bleb of an aneurysm is exposed to a shear stress higher than that of any other measured point. Wall shear stress is a dynamic frictional force induced by a viscous fluid moving along a surface of solid material. The endothelium regulates local vascular tone by releasing vasodilator and vasoconstrictor substances (29, 34). It is sensitive to changes in oscillating wall shear stress, which has stronger biologic influence on vessels by impinging on various endothelial functions than direct mechanical force (29, 34). Increased wall shear stress is regarded as a major factor in the development and growth of cerebral aneurysms (27, 30). Increased wall shear stress caused by increased flow velocity stimulates the release of endothelium-derived nitrous oxide, which is known as a strong vasodilator and also is a potential factor in arterial wall degeneration (27, 28, 34, 35). Therefore, a local increase in wall shear stress may cause local dilatation and degeneration of arterial walls.

Limitations of CFD

Any simulation study is based on a number of simplifying assumptions, such as considering blood as a Newtonian fluid, ignoring the real thickness of the aneurysmal wall, neglecting effect of gravity and position, and others. The validity of these assumptions seem to be of secondary importance compared with the influence of the geometry and the pulsating nature of blood flow; these are the most important factors for predicting possible aneurysmal growth and rupture.

In addition to the model assumptions, another limitation of computational analysis is that it is not possible, with current computer resources and time limitations in clinical practice, to evaluate the influence on the aneurysm hemodynamics of all model parameters (eg, heart rate and rhythm, blood pressure) and their variations in time. Although computer modeling allows for easy manipulation of these parameters, at present we usually deal with a few representative cases revealing only the most essential hemodynamic features of the aneurysm under study. Full parametric studies are rarely done. It is also wise to be aware of the actual accuracy of different stages of computer simulation and to keep it consistent. For instance, it may not make sense to compute flow fields accurate to 1% if the input geometry is accurate to only 10%.

Model validation is an essential, ever-present component of CFD simulation work. Any opportunity to compare fluid dynamic data from laboratory and clinical studies with simulations should not be neglected. This is especially important for patient-specific analysis in which faithful representation of the geometry is required to achieve meaningful results. As stated in reference 36, "improvements in laboratory and clinical fluid dynamic measurement capabilities can have a direct, positive impact on the accuracy and usefulness of CFD simulations by helping to identify the relevant sources of error so improvements could be made."

Models of Rigid and Deformable Vessels

Simulations with deformable vessels are more realistic, from a general point of view. However, their major disadvantage is a long computational time (more than an average of 7 days for the cases presented in Figure 4). Another restriction is the limited number of elastic models available in commercial CFD codes. For instance, linear homogeneous elastic behavior of the wall is the only option currently available in Fidap. Nevertheless, studies such as those in Figure 4 may provide a basic understanding of the hemodynamic behavior of geometrically similar intracranial aneurysms. It is reasonable to expect the eventual elimination of these deficiencies with further progress in both computer hardware and software.

Conclusion

This study was concerned with developing an efficient technique for the automatic creation of vascular computer replicas from medical imaging sources. We sought a practical method that neurosurgeons or neuroendovascular surgeons could use. Such a technique should simplify the geometry under consideration to decrease the computational time needed for CFD analysis and still preserve the essential features. Although we were mainly interested in cerebral aneurysms, this approach can also be used for other conditions, such as arteriovenous malformations

(AVMs), AVM flow-induced aneurysms, and atherosclerosis in intracranial and extracranial vessels, among others. Patient-specific computer modeling, combined with information from other imaging modalities, may provide important insight into flow dynamics before and after surgical or endovascular treatment.

Acknowledgments

We express our deep thanks to Mr Hiroyuki Shimura, Graphics System Analyst, SGI Japan, and Ms Midori Ooki, Research Center of Computational Mechanics Inc, Tokyo, Japan for their help in fulfilling this work.

References

1. Forget TR, Benitez R, Veznedaroglu E, et al. **A review of size and location of ruptured aneurysms.** *Neurosurgery* 2001;49:1322–1326
2. Steiger HJ, Liepsch DW, Poll A, et al. **Hemodynamic stress in terminal saccular aneurysms: a laser Doppler study.** *Heart Vessels* 1988;4:162–169
3. Steiger HJ, Poll A, Liepsch DW, et al. **Hemodynamic stress in terminal aneurysms.** *Acta Neurochir (Wein)* 1988;93:18–23
4. Tateshima S, Murayama Y, Villablanca P, et al. **Intraaneurysmal flow dynamics study featuring an acrylic aneurysm model manufactured using a computerized tomography angiogram as a mold.** *J Neurosurg* 2001;95:1020–1027
5. Imbesi SG, Kerber CW. **Analysis of slipstream flow in two ruptured intracranial cerebral aneurysms.** *AJNR Am J Neuroradiol* 1999;20:1703–1705
6. Kerber CW, Imbesi SG, Knox K. **Flow dynamic in a lethal anterior communicating artery aneurysm.** *AJNR Am J Neuroradiol* 1999;20:2000–2003
7. Hazama F, Hashimoto N. **An animal model of cerebral aneurysms.** *Neuropathol Appl Neurobiol* 1987;13:77–90
8. Burleson AC, Strother CM, Turitto VT. **Computer modeling of intracranial saccular and bifurcating aneurysms for the study of their hemodynamics.** *Neurosurgery* 1995;37:774–784
9. Canham PB, Ferguson GG. **A mathematical model for the mechanics of saccular aneurysms.** *Neurosurgery* 1985;17:291–295
10. Foutrakis GN, Burgreen G, Yonas H, et al. **Construction of 3D arterial volume meshes from magnetic resonance angiography.** *Neurol Res* 1996;18:354–360
11. Foutrakis GN, Yonas H, Sclabassi RJ. **Finite element methods in the simulation and analysis of intracranial blood flow.** *Neurol Res* 1997;19:174–186
12. Foutrakis GN, Yonas H, Sclabassi RJ. **Saccular aneurysm formation in curved and bifurcating arteries.** *AJNR Am J Neuroradiol* 1999;20:1309–1317
13. Gonzalez CF, Cho YI, Ortega HV, et al. **Intracranial aneurysms: flow analysis of their origin and progression.** *AJNR Am J Neuroradiol* 1992;13:181–188
14. Low M, Perktold K, Raunig R. **Hemodynamics in rigid and distensible saccular aneurysms: a numerical study of pulsatile flow characteristics.** *Biorheology* 1993;30:287–298
15. Perktold K, Peter R, Resch M. **Pulsatile non-Newtonian blood flow simulation through a bifurcation with an aneurysm.** *Biorheology* 1989;26:1011–1030
16. Milner JS, Moore JA, Rutt BK, Steinman DA. **Hemodynamics of human carotid artery bifurcations: computational studies with models reconstructed from magnetic imaging of normal subjects.** *J Vasc Surg* 1998;27:143–156
17. Batnitzky S, Price HI, Cook PN, Cook LT, Dwyer III SJ. **Three-dimensional computer reconstruction from surface contours for head CT examinations.** *J Comput Assist Tomogr* 1981;5:60–67
18. Di Martino ES, Guadagni G, Fumero A, et al. **Fluid-structure interaction within realistic three-dimensional models of the aneurysmatic aorta as a guidance to assess the risk of rupture of the aneurysm.** *Med Eng Phys* 2001;23:647–655
19. Myers JG, Moore JA, Ojha M, Johnston KW, Ethier CR. **Factors influencing blood flow patterns in the human right coronary artery.** *Ann Biomed Eng* 2001;29:109–120
20. Gorniak RJT, Kramer EL, Meguire GQ Jr, Noz ME, Schettino CJ, Zeleznik MP. **Evaluation of semiautomatic 3D fusion technique applied to molecular imaging and MRI brain/volume data sets.** *J Med Systems* 2003;27:141–156
21. Parsai EI, Ayyangar KM, Dobelbower RR, Siegel JA. **Clinical fusion of three-dimensional images using Bermsstrahlung SPECT and CT.** *J Nucl Med* 1996;38:319–324
22. Ladak HM, Milner JS, Steinman DA. **Rapid three-dimensional segmentation of the carotid bifurcation from serial MR images.** *J Biomech Eng* 2000;122:96–99
23. Fluent Incorporated Website. *Fidap Theory Manual.* Available at: http://www.unc.edu/atn/asg/applications/fluent/fidap8.7.2/documentation.
24. Anderson GB, Findlay JM, Steinke DE, et al. **Experience with computed tomographic angiography for the detection of intracranial aneurysms in the setting of acute subarachnoid hemorrhage.** *Neurosurgery* 1997;41:522–528
25. Anderson GB, Steinke DE, Petruk KC, et al. **Computed tomographic angiography versus digital subtraction angiography for the diagnosis and early treatment of ruptured intracranial aneurysms.** *Neurosurgery* 1999;45:1315–1322
26. Moore JA, Steinman DA, Ethier CR. **Computational blood flow modeling errors associated with reconstructing finite element models from magnetic resonance imaging.** *J Biomech* 1998;31:179–184
27. Fukuda S, Hashimoto N, Naritomi H, et al. **Prevention of rat cerebral aneurysm formation by inhibition of nitric oxide synthtase.** *Circulation* 2000;102:2532–2538
28. Geng Y, Hannson GK, Holme E. **Interferon-gamma and tumor necrosis factor synergize to induce nitric oxide production and inhibit mitochondrial respiration in vascular smooth muscle cells.** *Circ Res* 1992;71:1268–1276
29. Luscher TF, Tanner FC. **Endothelial regulation of vascular tone and growth.** *Am J Hypertens* 1993;6:283S–293S
30. Rossitti S. **Shear stress in cerebral arteries carrying saccular aneurysms: a preliminary study.** *Acta Radiol* 1998;39:711–717
31. Hassan T, Ezura M, Timofeev E, et al. **Computational simulation of therapeutic parent artery occlusion to treat giant vertebrobasilar aneurysm.** *AJNR Am J Neuroradiol* 2004. In press.
32. Hassan T, Timofeev E, Ezura M, et al. **Hemodynamic analysis of an adult vein of Galen aneurysmal malformation using 3D image based computational fluid dynamics.** *AJNR Am J Neuroradiol* 2003;24:1075–1082
33. Steinman DA, Milner JS, Noreley CJ, Lownie SP, Holdsworth DW. **Image-based computational simulation of flow dynamics in a giant intracranial aneurysm.** *AJNR Am J Neuroradiol* 2003;24:567–578
34. Stamler JS. **Redox signaling: nitrosylation and related target interactions of nitrous oxide.** *Cell* 1994;78:931–936
35. Guzman RJ, Abe K, Zarins CK. **Flow-induced arterial enlargement is inhibited by suppression of nitric oxide synthtase activity in vivo.** *Surgery* 1997;122:273–280
36. Metcalfe RW: **The promise of computational fluid dynamics as a tool for delineating therapeutic options in the treatment of aneurysms [editorial].** *AJNR Am J Neuroradiol* 2003;24:553–554

超急性期治療の最前線
-血栓溶解療法を中心に-

国立循環器病センター内科脳血管部門　髙田　達郎

KEY WORDS
●血栓溶解療法
●局所線溶療法
●tissue plasminogen activator

Up to date hyperacute therapy of ischemic stroke
-mainly on thrombolytic therapy-
Tatsuro Takada

はじめに

虚血性脳血管障害の治療は，1995年のNational Institute of Neurological Disorder and Stroke (NINDS) rt-PA Stroke Studyの報告を境に大きく変わった。すなわち発症3時間以内の超急性期虚血性脳血管障害に対するrecombinant tissue plasminogen activator (t-PA)静注法の有効性が示され[1]，翌年に米国食品医薬品局(FDA)で認可，現在は世界各国で行われるようになった。また，1999年には発症6時間以内の中大脳動脈閉塞症を対象としたPROACT Ⅱ (Prolyse in Acute Cerebral Thromboembolism Ⅱ) studyによる局所線溶療法の効果も報告され[2]，虚血性脳血管障害は「Brain attack」として超急性期治療の重要性が叫ばれるようになった。最近では超音波を併用した血栓溶解療法や異物除去deviceを用いた血栓除去法なども試みられるようになり，また，MRIによる超急性期画像診断の発達により，より安全で効果の高い治療法が模索されている。本稿では，血栓溶解療法を中心に，超急性期治療の現状について解説する。

Ⅰ．血栓溶解療法の根拠

脳梗塞症例のなかには発症後数時間から一両日のうちに症状が劇的に改善するものがある。この現象はspectacular shrinking deficit (SSD)と呼ばれている。Minematsuら[3]は，SSDが広汎な虚血症候で発症した脳塞栓症例の10%強にみられることを報告し，SSDの機序として栓子の溶解に伴う脳組織の早期再灌流を推定した。また，CT，MRIなどの画像診断機器の発達や脳虚血病態の解明も進み，梗塞巣が完成する以前の発症3～6時間以内に血流を再開することにより，脳梗塞への進展を防止あるいは軽減できることも示された。

以上より，虚血性脳血管障害における超急性期とは，画像上も明らかな脳梗塞巣を指摘できず，脳虚血が可逆的

で，治療により症候の改善が見込める，発症より3～6時間以内程度の時期と定義できる。

Ⅱ．血栓溶解療法の変遷

血栓溶解療法の歴史は古く，すでに1960年代に試みられていた。しかし，当時の血栓溶解療法はCTによる脳出血の除外ができず，使用された血栓溶解薬も第1世代といわれるストレプトキナーゼ(SK)などで，血栓への親和性が低く，流血中のplasminogenをplasminに変換するため，全身性の線溶状態を惹起しやすく，また，血栓到達までに大半が失活するために，血栓溶解作用も弱く，大量投与の必要があった。さらに投与時期も比較的遅いものであったため，出血性合併症の頻度が非常に高かった。しかし，1980年代にt-PAなどの血栓親和性が高く，血栓溶解作用の強い第2世代が開発，実用化され，さらに画像診断により治療効果の高い症例の選択が可能となったことで，本療法は1980年代後半より再び脚光をあびることとなった。1990年中～後半にかけて欧米よりt-PA静注法による無作為化比較試験(randomized controlled trial；RCT)が相次いで報告され，今日に至っている[1)2)4)-9)]。

一方で，動脈内投与，特に血栓溶解薬を直接血栓内に投与する局所線溶療法も1980年代後半より試みられるようになった[10)11)]。1999年，線溶療法に関するはじめてのRCTであるPROACTⅡstudyの結果が報告された[2)]。さらに近年は血栓親和性の向上や血中半減期の延長による効果の増強を図った第3世代t-PAや脳保護薬，抗GⅡb/Ⅲa薬や超音波との併用，異物除去deviceによる血栓除去法の試みなど血栓溶解療法の新しい展開が始まりつつある。

Ⅲ．日本の現状

わが国では，1970年代前半にウロキナーゼ(UK)少量点滴静注法の検討が行われ，発症3日以内の脳梗塞に有効とされた。しかし，その投与方法，投与量からは血栓溶解という観点での効果は疑問視されてきた。1993年，Yamaguchiら[12)]は世界に先駆け，発症6時間以内の超急性期脳塞栓症に対してのt-PA(デュテプラーゼ)静注法の有効性を報告した。しかし，本薬剤の特許権をめぐる争いのため製造中止となった。その後もt-PAは未承認のままで，海外よりかなり立ち後れた感は否めず，大部分の施設では超急性期といえども保存的加療に終止せざるをえないのが実情であった。脳神経外科を中心としたごく一部の施設では，超急性期の血栓溶解療法としてUKによる局所線溶療法が施行されてきた。平成12年度厚生科学研究費補助金健康科学総合研究事業「脳梗塞急性期医療の実態に関する研究」での1年間前向き登録では，UKによる局所線溶療法は登録解析患者の1.6%(発症6時間以内の3%)で行われた[13)]。2000年になり第3世代t-PA(パミテプラーゼ)の臨床試験が開始，2002年にUKによる局所線溶療法のRCT(MCA- Embolism Local Fibrinolytic Intervention Trial；MELT-JAPAN)[14)]，さらにアルテプラーゼ静注法の臨床試験も開始され，わが国においても超急性期虚血性脳血管障害の治療に新たな展開が生まれている。

Ⅳ．血栓溶解療法の実際

1．静注法

1)大規模臨床試験

表1に主な静注法の概要をまとめた。SK静注法は，オーストラリア，欧州で3件の試験が実施されたが，いずれもSK群で早期死亡や重篤な出血性合併症が有意に高く，すべての試験が途中で中止となった[4)-6)]。前述のわが国で実施された世界初のt-PA無作為化比較試験は，発症6時間以内の脳塞栓症例に対してデュテプラーゼ20MUが静脈内投与された。この結果，再開通率は有意に上昇し，1ヵ月目の転帰も改善傾向が認められた。また，症候性頭蓋内出血の発症率は偽薬群と差がなかった[12)]。西ヨーロッパ諸国での試験，ECASS Ⅰ(The European Cooperative Acute Stroke Study Ⅰ)では，1.1mg/kgのアルテプラーゼ静注法で検討された。対象全例の90日目の転帰には明らかな差はなかったが，プロトコール違反を除いた症例で検討すると，t-PAの治療効果が示されている。また，症候の回復時間と入院期間はt-PA群で短かったが，30日目の死亡率はプロトコール違反のあるt-PA群で非常に高く，t-PAの使用に際しては症例の厳密な選択が要求されることが明らかになった[7)]。この結果を踏まえて，投与量を0.9mg/kgに下げ，エントリー基準をより厳しくした再試験が実施された(ECASS Ⅱ)。modified rankin scaleスコア≦2の症例はプラセボ群46.0%に対しt-PA群54.3%で転帰良好例が有意に多かった。発症3時間以内と3～6時間での効果および出血性合併症に差はなかった[8)]。冒頭に述べたNINDS studyでは，3ヵ月後の転帰

表1．血栓溶解療法無作為化比較試験の概要

	症例数	投与開始時間	用量	有効性	症候性頭蓋内出血発症率
1．SK静注法					
ASK(1996)[4]	340	＜4時間	150万U	−	12.6%
MAST-E(1994)[5]	270	＜6時間	150万U	−	6.0%
MAST-I(1995)[6]	622	＜6時間	150万U	−	17.5%
2．t-PA静注法					
JTSG(1993)[12]	98	＜6時間	20MU(デュテプラーゼ)	+	8.5%
NINDS(1995)[1]	624	＜3時間	0.9mg/kg(アルテプラーゼ)	+	6.4%
ECASS-Ⅰ(1995)[7]	620	＜6時間	1.1mg/kg(アルテプラーゼ)	+/−	19.8%
ECASS-Ⅱ(1998)[8]	800	＜6時間	0.9mg/kg(アルテプラーゼ)	+/−	8.8%
ATLANTIS(1999)[9]	579	3～5時間	0.9mg/kg(アルテプラーゼ)	+/−	7.2%

良好例は，t-PA群で有意に高率であった(プラセボ群21%：t-PA群34%)。臨床病型による有効性の差はなかった[1]。ATLANTIS (Alteplase Thrombolysis for Acute Noninterventional Therapy in Ischemic Stroke)では，NINDSのプロトコールに従い発症3～5時間での有効性を検討したが，転帰改善効果は証明されなかった[9]。以上の結果を踏まえ，米国脳卒中協会(AHA)などからガイドラインが示されている[15]。わが国におけるアルテプラーゼ静注法の臨床試験では，発症3時間以内の虚血性脳血管障害102例に対して，0.6mg/kgの投与量で実施され，有効性，安全性ともNINDS studyに遜色ない結果を示した[16]。

2)治療の実際

静注法に関しては，適応症例や投与方法などがガイドラインとして明確化されている。表2にAHAのガイドラインを示した。

(1)適応症例の選択

症例の選択にあたっては，有効性が十分に期待でき，しかも安全に行えるかがポイントになる。血栓溶解療法の最大の問題点は，症候性頭蓋内出血の増加である。SKは症候性頭蓋内出血の合併率が約12～17%と非常に高く，むしろ禁忌といえる[4)-6)]。また，t-PAによる頭蓋内出血は6～17%で，最も頻度の高かったECASSⅠでの合併例を除くと6～8%である[1)7)-8)]。1997年，FDAの要請による全米57施設での389人を対象とした第Ⅳ相試験(STARS研究)が実施され，症候性頭蓋内出血の合併率は3.3%であった。プロトコール違反は32.6%に認められ，その内訳は発症3時間以降での投与(13.4%)，24時間以内の抗血小板薬治療(6.7%)，収縮期血圧＞185Torr (3.3%)であった[17]。ガイドラインからの逸脱例が多く含まれているKatzanら[18]の報告(プロトコール違反が50%)では，症候性頭蓋内出血性の合併率が15.7%に達し，治療群とコントロール群に転帰の差がなかった。しかし，NINDS研究に習熟した実施者によるSTARSよりKatzanらの報告のほうが臨床での実情に近いという意見もある。Levyら[19]は，症候性頭蓋内出血の危険因子として，治療前高血圧をあげた。すなわち，治療前拡張期血圧100mmHg以上の群の症候性頭蓋内出血発生頻度は100mmHg未満の群の18倍と著しく高頻度であった。その他，糖尿病の合併，高齢者や重篤な臨床症候を有する例，CT上，early ischemic sign(脳溝消失，基底核構造の不鮮明化など)を呈する例，また，治療前に抗血小板薬や抗凝固薬内服中であった患者は注意を要する。

(2)投与方法

現在使用可能なt-PAは，血中半減期が非常に短く，有効な血栓溶解効果を得るためには点滴投与が必要である。海外の臨床試験での投与量は，おおむね0.9mg/kg(最大90mg)で，この10%をボーラスで投与し，残りを1時間の点滴投与としている。

(3)治療後管理

AHAのガイドライン[15]によると，t-PA投与後24時間までは厳重な集中治療管理が必要とされている。そのポイントは，①高血圧時(収縮期＞180mmHg，拡張期＞105mmHg)の降圧療法(静脈内投与)，②中心静脈カテーテル，動脈穿刺，胃管および膀胱カテーテルの制限，③抗血小板薬，抗凝固薬投与の禁止である[2]。NINDS studyでは症候性頭蓋内出血の合併はほとんど36時間以内に発症し，特にt-PA投与後の臨

表2．AHAガイドラインの概要

① 対象症例：発症3時間以内の虚血性脳血管障害
② 投与方法：recombinant t-PA 0.9mg/kg(最大90mg)全体の10％を急速静注し，残りを60分で点滴静注
③ 投与前のCT：出血やearly CT sign*がないことを確認する
④ 除外項目
 1)経口抗凝固療法中で，INRが1.7以上
 2)過去48時間以内にヘパリンを使用し，APTTが延長しているもの
 3)血小板数＜10万/mm³
 4)過去3ヵ月以内の脳卒中または重症頭部外傷
 5)過去14日以内の手術
 6)治療前血圧が収縮期＞185mmHg，拡張期＞110mmHg
 7)神経症候の急速な改善
 8)単独かつ軽度の神経症候(失調，感覚障害，構音障害，わずかな脱力)
 9)頭蓋内出血の既往
 10)過度の低血糖(＜50mg/dL)，高血糖(＞400mg/kg)
 11)発症時の痙攣発作
 12)過去21日以内の消化管または尿路系出血
 13)最近の心筋梗塞
⑤ 集中管理，治療の行える施設内で実施する
⑥ NIH Stroke Scaleが23点以上の重症例は注意が必要である
⑦ 治療開始前に，予想される効果と危険性を本人，家族に十分に伝え，相談すること
⑧ 治療後24時間の集中管理
 1)高血圧時(収縮期＞180mmHg，拡張期＞105mmHg)には降圧薬の静脈投与
 2)中心静脈ルートの確保や動脈穿刺の制限
 3)t-PA投与中および投与後30分間は膀胱カテーテル留置を行わない
 4)治療後24時間以内は胃カテーテル挿入もできるだけ避ける
 5)治療後24時間以内は抗血小板薬，抗凝固薬などの投与を行わない
⑨ その他
 1)治療後の神経学的悪化の際には，CTにより頭蓋内出血の有無を診断する
 2)出血性合併症に対しては，t-PA投与の中止，血液凝固系検査を行い，必要に応じて輸血，新鮮血漿や血小板輸血，外科的処置を行う

＊：大脳動脈支配領域の33％以上の低吸収域，浮腫性変化，脳溝の消失
(文献[15]より引用，一部改変)

床症候改善が認められない場合は注意を要する。

(4)今後の課題

血栓溶解療法は，厳格なガイドラインの遵守により比較的安全で良好な治療結果をもたらす。しかし，厳格であるがゆえにt-PA投与例は米国においても脳梗塞患者全体の1～2％，中核的施設においてでも5％程度を占めるにすぎないといわれている[20]。血栓溶解療法の恩恵を受けられる患者は決して多いとはいえず，静注法の限界を示しているともいえる。発症3時間以降での有効性に関しては，NINDS，ECASSを対象としたメタ解析では，発症6時間以内でのt-PA静注法の有効性も否定できないといわれた[21]。NINDS研究とほぼ同様のプロトコールで発症6時間以内の脳梗塞6,000例を対象とした大規模RCTが開始されている[22]。

2．局所線溶療法

1)大規模臨床試験

局所線溶療法の大規模RCTとしては，前述のPROACTⅡが唯一である。本試験は，マイクロカテーテルによるプロUK 9 mg局所動脈内投与に関する試験である。再開通率はプロUK群で66％とコントロール群に比べ明らかに高く，90日目のmodified rankin scale 2以下の転帰良好例はプロUK群40％，コントロール群25％であった。一方，症候性頭蓋内出血はコントロール群2％に対してプロUK群10％と高率であった[2]。なお，本研究に対しては症例数が少ないとの批判もあり，FDAの認可には至っていない。2002年より開始されたわが国におけるRCTである「超急性期脳塞栓症に対する局所線溶療法の効果に関する臨床研究(主任研究者 小川彰)」(MELT-JAPAN)では，血栓溶解薬としてUK(最大量60万単位)を用い，発症6時間以内の中大脳動脈塞栓症に対する有効性を検討している。発症3ヵ月目の自立度(modified rankin scaleスコア≦2)を一次評価項目として，治療群100例，対照群100例を目標とした[14]。詳細は，MELT-JAPANのホームページを参照されたい(http://melt.umin.ac.jp/)。

2)治療の実際

現在のところ局所線溶療法のガイドラインは存在せず，適応基準，方法，投与薬剤などは施設間で異なるのが現状である。前述したMELT-JAPANでは，この問題を解決するため治療手技についても標準化を行っている。MELT-JAPANでのプロトコールを中心に述べる(表3)[14]。

(1)適応症例の選択

通常，本治療における適応時間は静注法のそれより長く，6時間以内に薬剤投与可能な症例が対象となる場合が多い。その他はほぼ静注法に準じてい

表3．MELT-JAPANの概要

① 目的
虚血性脳血管障害超急性期患者に対する局所線溶療法の有用性と安全性を一般的治療法を対照として多施設共同ランダム化比較試験で検証する。

② 対象
1）中大脳動脈閉塞(M1あるいはM2)。
2）発症時刻が特定可能で発症6時間以内に局所線溶療法を開始できる患者。
3）CTでまったく変化を認めないか，病側に軽微な初期虚血変化(島皮質，前頭・側頭弁蓋部に限局する球種内のわずかな低下やシルビウス裂の消失，レンズ核の不鮮明化)のみを認めるもの。ただし，CT撮像後より2時間以内に本療法を開始できる患者。
4）年齢20歳以上75歳以下。
5）4＜NIHSSスコア＜23。
6）性別は問わない。

③ 除外項目
a．臨床的除外項目
1）昏睡(Japan coma scale 100以上)。
2）発症時痙攣。
3）3ヵ月以内の完成型脳卒中の既往(一過性脳虚血発作を除く)。
4）出血性リスクの除外。
①30日以内の手術，生検，臓器損傷を伴う外傷
②2週間以内の臓器出血(消化管出血，尿路出血，後腹膜出血など)
③3ヵ月以内の重症頭部外傷
④血小板数＜100,000/mm³などの出血性素因
⑤抗凝固療法中(INR＞1.7)
5）治療抵抗性の高血圧(SBP＞180mmHg，DBP＞100mmHg)。
6）授乳中，妊娠またはその可能性がある。
7）その他，担当医師が不適当と判断した。

b．CTによる除外項目
1）あらゆる頭蓋内出血。
2）頭蓋内腫瘍。
3）脳動脈瘤，脳動静脈奇形他，脳静脈血栓症の疑われる患者。

c．脳血管撮影による除外項目
1）MCA以外に閉塞を認める患者。
2）もやもや病，動脈解離の患者。
3）動脈閉塞が確認できない患者。
4）閉塞部位より中枢側に高度の動脈狭窄を認め，マイクロカテーテルが通過困難と考えられる患者。
5）脳動脈瘤が認められた患者。

④ 治療手技および方法
1）大腿動脈経由，6Fr。シース留置を原則として用いる。
2）導入用カテーテルを導入する前に全身ヘパリン化を行う。投与量は5,000単位とし追加しない。
3）局所線溶療法手技については，線溶療法を基盤としつつ簡単な血管内手技を加えることとする。
4）血管撮影を施行する。
5）全身ヘパリン化を行う。
6）マイクロカテーテル先端を閉塞部位より遠位に置く。
7）ウロキナーゼ60万単位を生理的食塩水50mLに溶解したものを，シリンジポンプを用いて12万単位/10mLを5分間で注入する。注入終了時に導入用カテーテルからコントロールの血管撮影を行う。
8）治療後血管撮影。

(文献[14]より抜粋，一部改変)

るが，脳血管撮影による責任血管の閉塞を確認する必要があり，MELT-JAPANでは，中大脳動脈主幹部閉塞のみを対象とした。また，施設によっては血栓性機序による閉塞も含めている場合があるが，MELT-JAPANでは塞栓性機序のみを対象としている。

(2)投与方法

マイクロカテーテルによる閉塞局所での薬剤注入が原則である。注入部位は血栓近位，血栓内，血栓遠位がある。また注入方法として，手動あるいはシリンジポンプなどによる機械的注入方法があり，MELT-JAPANでは血栓遠位よりの機械的注入法による薬剤注入を行っている。使用薬剤としてはUK，t-PAなどがあるが，MELT-JAPANでは最大60万単位のUKを使用している。

(3)治療後管理

静注法に準ずる。脳血管撮影上，再開通を得られなかった症例は頭蓋内出血の発症に十分注意する。降圧療法に関しては，再開通の有無に関わらず，収縮期血圧で180mmHgをめどに持続点滴静注による降圧を図っている。また，治療24時間後までの抗血栓療法は禁忌となり，治療24時間以降のCTにて梗塞範囲，出血性梗塞の有無を確認，可能であれば再発予防目的でヘパリン10,000～15,000単位/日の持続点滴静注などの抗血栓療法を開始する。

V．今後の展望

t-PAの開発以来，虚血性脳血管障害は治療可能な疾患として大きな関心が寄せられるようになった。しかし，劇的な効果が期待できる反面，重篤な出血性合併症を伴うこともあり，本療法はいわば「諸刃の剣」としての性格を

もっている。その適応症例の選択，治療前後の管理に誤りがあれば，治療効果が期待できないばかりか，逆に患者の予後を悪化させる可能性もある。本治療法を安全に行うためには，虚血性脳血管障害の病態，診断，治療などについて熟知していなければならない。近年，この問題を解決すべくいくつかの試みが行われている。第1は，前述した血栓親和性の向上や血中半減期の延長による効果の増強を図った第3世代t-PAの開発とその実用化である。第2は，脳保護薬や超音波との併用療法である[23)-25)]。第3は，異物除去deviceや経皮的血管拡張術などの脳血管内治療手技である[26)-28)]。一方，MRIなどの画像診断機器を用いて適応判定をより的確に行い，症候性頭蓋内出血の減少や適応時間の延長をもたらそうとする試みもある[29)]。

しかし，現時点では血栓溶解療法の恩恵を受けることのできる患者は，虚血性脳血管障害患者の一部に過ぎない。わが国の有床医療機関への発症6時間以内入院は虚血性脳血管障害の28％に過ぎず[13)]，この問題の解決のためには，より多くの患者が早期に診療を受けることを可能とする診療体制の再構築と的確な診断・治療を実践できる脳卒中専門医の育成が急務といえる。また，各種メディアを介した宣伝・啓発，非専門医療職への講習，救急搬送システムの整備も必要となろう。これらの結果によって，多くの脳卒中患者がこの恩恵を受けられるようになることを期待したい。

文　献

1) The National Institute of Neurological Disorders and Stroke rt-PA Stroke Study Group : Tissue plasminogen activator for acute ischemic stroke. N Engl J Med 333 : 1581－1587, 1995
2) Furlan A, Higashida R, Wechsler L, et al : Intra-arterial prourokinase for acute ischemic stroke. JAMA 282 : 2003－2011, 1999
3) Minematsu K, Yamaguchi T, Omae T : 'Spectacular shrinking deficit' : A rapid recovery from a major hemispheric syndrome by migration of an embolus. Neurology 42 : 157－162, 1992
4) Donnan GA, Davis SM, Chambers BR, et al : Streptokinase for acute ischemic stroke with relationship to time of administration : Australian Streptokinase (ASK) Trial Study Group. JAMA 276 : 961－966, 1996
5) Hommel M, Boissel JP, Cornu C, et al : Termination of trial of streptokinase in severe acute ischaemic stroke. Lancet 345 : 57, 1994
6) Multicenter Acute Stroke Trial-Italy (MAST-I) Group : Randomised controlled trial of streptokinase, aspirin, and combination of both in treatment of acute ischaemic stroke. Lancet 346 : 1509－1514, 1995
7) Hacke W, Kaste M, Fieschi C, et al : Intravenous thrombolysis with recombinant tissue plasminogen activator for acute hemispheric stroke. The European Cooperative Acute Stroke Study (ECASS). JAMA 274 : 1017－1025, 1995
8) Hacke W, Kaste M, Fieschi C, et al : Randomised double-blind placebo-controlled trial of thrombolytic therapy with intravenous alteplase in acute ischemic stroke (ECASS Ⅱ). Second European-Australasian Acute Stroke Study Investigators. Lancet 352 : 1245－1251, 1998
9) Clark WM, Wissman S, Albers GW, et al : Recombinant tissue-type plasminogen activator (Alteplase) for ischemic stroke 3 to 5 hours after symptom onset. The ATLANTIS Study : a randomized controlled trial. Alteplase Thrombolysis for Acute Noninterventional Therapy in Ischemic Stroke. JAMA 282 : 2019－2026, 1999
10) Gonner F, Remonda L, Mattle H, et al : Local intra-arterial thrombolysis in acute ischemic stroke. Stroke 29 : 1894－1900, 1998
11) Zeumer H, Freitag HJ, Zanella F, et al : Local intra-arterial fibrinolytic therapy in patients with stroke : urokinase versus recombinant tissue plasminogen activator (r-TPA). Neuroradiology 35 : 159－162, 1993
12) Yamaguchi T, Hayakawa T, Kikuchi H, et al : Intravenous tissue plasminogen activator ameliorates the outcome of hyperacute embolic stroke. Cerebrovasc Dis 3 : 269－272, 1993
13) 山口武典：脳梗塞急性期医療の実態に関する研究．平成12年度厚生科学研究費補助金による健康科学総合研究事業研究報告書．大阪，国立循環器病センター，29－30，2001
14) 小川　彰：超急性期脳塞栓症に対する局所線溶療法の効果に関する臨床研究．平成13年度厚生科学研究費補助金による21世紀型医療開拓推進研究事業報告書．岩手，岩手医科大学医学部，15－28，2002
15) Adams HP, Brott TG, Furlan AJ, et al : Guidelines for thrombolytic therapy for acute stroke ; A supplement to the guidelines for management of patients with acute ischemic stroke ; A statement for health care professionals from a special writing group of the Stroke Council, American Heart Association. Stroke 27 : 1711－1718, 1996
16) 峰松一夫，山口武典，端　和夫，他：発症3時間以内の虚血性脳血管障害に対するGMK-527(アルテプラーゼ)静注療法臨床試験の結果．脳卒中 26 : 139, 2004
17) Albers GW, Bates VE, Clark WM, et al : Intravenous tissue-type plasminogen activator for treatment of acute stroke : The Standard Treatment with Alteplase to Reverse Stroke (STARS) study. JAMA 238 : 1145-1150, 2000
18) Katzan IL, Furlan AJ, Lloyd LE, et al : Use of tissue-type plasminogen activa-

tor for acute ischemic stroke : The Cleveland area experience. JAMA 283 : 1151−1158, 2000
19) Levy DE, Brott TG, Haley EC, et al : Factors related to intracranial hematoma formation in patients receiving tissue-type plasminogen activator for acute ischemic stroke. Stroke 25 : 291−297, 1994
20) Chiu D, Krieger D, Villar-Cordova C, et al : Intravenous tissue plasminogen activator for acute ischemic stroke. Feasibility, safety, and efficacy in the first year of clinical practice. Stroke 29 : 18−22, 1998
21) Ringleb PA, Schellinger PD, Schranz, et al : Thrombolytic therapy within 3 to 6 hours after onset of ischemic stroke useful or harmful? Stroke 33 : 1437−1441, 2002
22) Hand P, et al : The third International Stroke Trial (IST-3) . Stroke 31 : 2866, 2000
23) Eggers J, Koch B, Meyer K, et al : Effect of ultrasound on thrombolysis of middle cerebral artery occlusion. Ann Neurol 53 : 797−800, 2003
24) Alexandrov AV : Ultrasound-enhanced thrombolysis for stroke : clinical significance. Eur J Ultrasound 16 : 131−140, 2002
25) Qureshi AI, Siddiqui AM, Suri MF, et al : Aggressive mechanical clot disruption and low-dose intra-arterial third-generation thrombolytic agent for ischemic stroke : a prospective study. Neurosurgery 51 : 1319−1327, 2002
26) Wikholm G : Transarterial embolectomy in acute stroke. AJNR Am J Neuroradiol 24 : 892−894, 2003
27) Kerber CW, Barr JD, Berger RM, et al : Snare retrieval of intracranial thrombus in patients with acute stroke. J Vasc Interv Radiol 13 : 1269−1274, 2002
28) Schumacher HC, Meyers PM, Yavagal DR, et al : Endovascular mechanical thrombectomy of an occluded superior division branch of the left MCA for acute cardioembolic stroke. Cardiovasc Intervent Radiol 26 : 305−308, 2003
29) Jansen O, Schellinger P, Fiebach J, et al : Early recanalisation in acute ischemic stroke saves tissue at risk defined by MRI. Lancet 353 : 2036 − 2037, 1999

＜新治療法＞
血栓溶解薬・抗血栓薬（t-PA とラジカルスカベンジャー）

血栓溶解療法：update

森　悦朗
東北大学大学院医学系研究科高次機能障害学

Key words：脳梗塞，血栓溶解療法：臨床試験
（脳卒中 26：647—650，2004）

はじめに

血栓溶解療法は，血栓溶解薬を生体内に投与して病的血栓を溶解し，虚血組織を再還流する治療法である．虚血性脳血管障害に対する血栓溶解療法は，1996 年米国において発症 3 時間以内の遺伝子組み換え組織プラスミノーゲン・アクチベーター（rt-PA；recombinant tissue plasminogen activator）による血栓溶解療法が承認されてから国際的にも拡がりつつある[1)2)]．本邦では，脳梗塞に対する血栓溶解療法は承認されておらず，現在，臨床試験が進行している．ここでは本邦で現在進行中の 2 つの血栓溶解療法の臨床試験，すなわち虚血性脳血管障害に対する rt-PA 静脈内投与の試験（Japan Alteplase Clinical Trial：J-ACT）および中大脳動脈塞栓症に対するウロキナーゼ局所動脈内投与の試験（Middle Cerebral Artery Embolism Local Fibrinolytic Intervention Trial：MELT Japan）の研究デザインや進捗状況を紹介するとともに，血栓溶解療法を踏まえた急性期虚血性脳血管障害の治療戦略を考えてみる．

脳梗塞に対する血栓溶解療法のエビデンス

脳梗塞に対する血栓溶解療法に関して高いレベルのエビデンスは，(1) 発症 3 時間以内の脳梗塞に対する遺伝子組み替え組織プラスミノーゲン・アクチベーター（rt-PA；recombinant tissue plasminogen activator）の経静脈的血栓溶解療法[1)2)]，(2) 発症 6 時間以内の中大脳動脈閉塞による脳梗塞に対するプロウロキナーゼ（Pro-UK）による局所動脈内血栓溶解療法[3)]の 2 つである．詳細は最近まとめた総説を参照されたい[4)]．

1995 年に報告された米国 National Institute of Neurological Disorders and Stroke（NINDS）試験は，rt-PA 経静脈的血栓溶解療法の無作為割付偽薬対照臨床試験である[2)]．発症 3 時間以内の脳梗塞に対する rt-PA（アルテプラーゼ）0.9mg/kg の静脈内全身投与（1 時間投与）が偽薬群と比較された．その結果，rt-PA 群で症候性頭蓋内出血の頻度は有意に増加（rt-PA 群 6.4% vs. 偽薬群 0.6%）したものの，3 カ月後の modified Rankin Scale（mRS）など複数の尺度で rt-PA 群が有意に良好であるという結果が示された．1996 年 6 月米国食品医薬局（FDA；Food and Drug Administration）は，上記の試験の結果を受けて rt-PA 経静脈的血栓溶解療法を承認した．これらの結果を受けて 3 時間以内治療法は現在では世界 40 カ国で承認され，使用が推奨されている．

1999 年に報告された Prolyse in Acute Cerebral Thromboembolism-II（PROACT-II）試験[3)]では，発症 6 時間以内の中大脳動脈閉塞による脳梗塞に対する超選択的カテーテルを用いたプロウロキナーゼ局所動脈内血栓溶解療法の有用性が検討された．その結果，プロウロキナーゼ群で閉塞血管の再開通率（プロウロキナーゼ群 66% vs. 偽薬群 18%）が有意に高く，機能評価尺度の日常生活自立（mRS＝0–2）の頻度（プロウロキナーゼ群 40% vs. 偽薬群 25%）も有意に高かった．プロウロキナーゼ群で症候性頭蓋内血腫の頻度（プロウロキナーゼ群 10% vs. 偽薬群 2.0%）は高かったが，有意差はなかった．PROACT-II の試験規模は充分大きくなかったため，米国 FDA はこの治療法の臨床使用を承認していない．

本邦においては，発症後 6 時間以内の内頚動脈系の塞栓性閉塞に対して 2,000 万あるいは 3,000 万単位の rt-PA（duteplase）または偽薬を 1 時間で経静脈的に投与する血管撮影を前提としたプロトコルの偽薬対照二重盲検試験が世界に先駆けて行われた[5)6)]．再開通は部

分再開通を含めて偽薬群に比べrt-PA投与群では有意に高いことが示され，また神経症候をhemispheric stroke scale（HSS）を用いた比較で，rt-PA投与群は偽薬群に比し有意に良好な改善を示していた．梗塞の出血性変化は出血性梗塞も脳内血腫形成も偽薬群とrt-PA投与群間に差はなかった．これらの研究はその後の血栓溶解療法の礎となったが，特許権の問題で本邦での実用化には至らなかった．

J-ACT

アルテプラーゼの静脈内投与法は発症後3時間以内の虚血性脳血管障害に対して確立した治療法であるが，本邦においては未承認である．日本人での有効性，安全性を確認する目的でJ-ACTは行われた．J-ACTは多施設共同によるオープン試験で，欧米ではアルテプラーゼ0.9mg/kgが用いられているが（10%を急速静注し，残りを1時間かけて持続点滴静注），過去日本で実施されたduteplaseによる臨床試験の結果報告を考慮し，0.6mg/kgの1用量が検討された．目標症例数は100例，主要評価項目は3カ月後のmRS 0–1の割合と，36時間以内の症候性頭蓋内出血発現頻度である．主要評価項目の目標数値は，既発表論文の系統的レビューとメタアナリシスによる加重平均値の90%信頼区間を設定することにより定めた．患者選択・除外基準，管理基準はNINDS試験[2]とAmerican Heart Association（AHA）Guidelines[1]に準拠されたが，CTにおいてearly ischemic changeがMCA支配領域の1/3を超えるもの，昏睡例（Japan Coma Scale 100以上），およびNIHSSが4以下の軽症例は除外された．

2002年4月から2003年9月に103例が登録された．患者背景に関して，発症から投与までの平均時間は150.5分，投与前NIHSSの平均値は15であり，病型比率を除いてNINDS試験Part 2と同様であった．有効性の主要評価項目とした発症3カ月後のmRS 0または1の割合は38例（36.9%）であり，計画で定めた評価の判断基準値33.9%を上回る結果であった．発症3カ月後のBI 100–95の割合は48.5%（NINDS試験Part2のアルテプラーゼ群50%，プラセボ群38%），発症24時間後のNIHSSが4点以上改善もしくは発症24時間でNIHSS 0点となった割合は49.5%（NINDS試験Part 1のアルテプラーゼ群47%，プラセボ群39%）であり，いずれもNINDS試験におけるアルテプラーゼ群の結果と同程度であり，副次評価項目の比較においても成績はNINDS試験のアルテプラーゼ群とほぼ同じ結果であった．

安全性における主要評価項目である投与開始後36時間以内の症候性頭蓋内出血の発現率は5.8%（6例）であり，事前に定めた評価の判断基準値9.6%を下回っていた．症候性頭蓋内出血を起こした6例のうち2例は出血性梗塞，4例は血腫で，うち3例に正中線偏位が認められた．出血性梗塞の1例と正中線偏位を伴った血腫の1例が死亡した．虚血性脳血管障害発症後90日までの死亡は10例であり，死亡率は9.7%であった．3日後までに4例が血管障害で死亡し，うち1例は0日後に脳内出血，その他3例は脳虚血により死亡した．他6例の死亡は11日後から87日後の間に起こった．本試験の死亡率は，公表論文のメタアナリシスにおける10～17%，またはNINDS試験におけるプラセボ群の21%より低値であった．これらの結果より，発症後3時間以内の虚血性脳血管障害患者に対しアルテプラーゼ0.6mg/kgを投与した場合，3カ月後の転帰および投与開始後36時間以内の症候性頭蓋内出血の発現率は海外での0.9mg/kg投与における公表論文と同程度であり，日本ではアルテプラーゼ0.6mg/kgの使用で北米や欧州での報告と同様の有効性，安全性が期待できると結論できる．

MELT Japan

局所線溶療法に関しては有用であるという主張が繰り返されているが，質の高いエビデンスは存在せず，有用性は未だ確立されていない．しかし現実には局所線溶療法は，最近の脳梗塞急性期治療の実態調査でも示されているように，すでにかなり多くの施設で様々な形で行われている．局所線溶療法を普遍的なものとして正当化できるほどのエビデンスは存在せず，局所線溶療法の利益を最大に引き出し，危険性を最小に抑える方法も確立されていない．MELT Japanは，厚生労働科学研究費の補助を受けて，局所線溶療法の有用性を検証することを目的に，虚血性脳血管障害超急性期患者に対するウロキナーゼを用いた局所線溶療法の有用性と安全性を一般的治療法を対照として多施設共同無作為ランダム化比較試験で検討するものである[7]．対象は発症6時間以内の中大脳動脈（M1またはM2）の塞栓症を対象にした局所線溶療法と一般的治療の無作為化対照比較試験である．ウロキナーゼは60万単位まで，マイクロカテーテルを介して閉塞局所に1時間以内で注入される．発症3カ月後のmRS 0～2（自立）にまで回復していることが主たるエンドポイン

トである．

2003年度末までに療法群に32例，対照群に33例が割り付けられた．療法群に割り付けられた例のうち31例が血栓溶解療法を受け，対照群の全例が一般的治療法を受けた．これらのうち3カ月間の試験期間を満了した，療法群の26例，対照群の26例を対象として中間解析を行った．療法群と対照群の間で背景および画像所見に，年齢など若干差がみられるものの有意に異なるものはなかった．療法群において，発症からウロキナーゼ投与開始までの時間は，平均227分，ウロキナーゼ投与量は，投与なし（1例），60万単位以下（9例），60万単位（16例）であった．カテーテルあるいはガイドワイヤーによる血栓の破砕は17例（65%）に行われていた．再開通は，なし4例，50%未満7例，50%以上14例，完全1例であった．死亡は，対照群で2/26例，療法群で1/26例であり，その差は有意ではなかった（p＝0.168）．24時間以内の症状悪化を伴う頭蓋内出血は，対照群で症候性出血性梗塞1例（3.8%），療法群では症候性出血性梗塞が2例，およびくも膜下＋脳内出血が1例（計11.5%）であり，療法群で多い傾向を示したが，その差は有意ではなかった（p＝0.132）．主たるエンドポイントであるmRS 0～2（自立）は対照群で8/26（30.8%），療法群で12/26（46.1%）であり，療法群に多い傾向を示したが，その差は有意ではなかった（p＝0.273）．これらの頻度は計画において想定した範囲内であった．なお副次的エンドポイントとしていたmodified Rankin Scale 0，1（障害なし）は，対照群で3/26（11.5%），療法群で10/26（38.5%）と，有意に療法群に多かった（p＝0.03）．2003年末までにエントリーされた対象数は，当初計画の1/3で対象集積の遅れがあるが，試験期間を延長し，試験を続行している[8]．

血栓溶解療法を踏まえた急性期虚血性脳血管障害の治療戦略

欧米ではアルテプラーゼ静脈内投与法の実際の臨床現場での検討も進み，適応対象が発症3時間以内であるため，この治療法を受ける患者は脳梗塞全体の10%にも満たないことが明らかにされている[9]．本邦においても発症3時間以内のrt-PA治療ガイドラインの選択基準を満たす症例は脳梗塞全体の7%と報告されている[10]．この率を上げるべく，患者および一般医家の教育，救急システムの改善を図ることが重要である．また最近は発症後3～6時間の例に対するアルテプラーゼ静脈内投与法の可能性に注目が集まっている．ECASS-I試験，ECASS-II試験，ATLANTIS試験を加えたメタアナリシス[11]では，rt-PA経静脈的血栓溶解療法は発症後3時間を超える例に対しても有用である可能性が示されている．

一方，臨床現場では選択基準に違反する症例に対してもrt-PA治療が行われているのが現状であり，選択基準を違反した症例にrt-PA治療を実施すると出血性合併症が増加する危険性が指摘されている[12][13]．急性期における的確な診断と患者選択，治療指針の遵守が副作用を減らす重要なポイントである．虚血性脳血管障害と血栓溶解療法に対して経験豊かな施設に患者を集中させるようなシステムを構築すべきかも知れない．このことは訓練を行う点でも重要であろう．

文　献

1) Adams HP Jr, Brott TG, Furlan AJ, et al : Guidelines for Thrombolytic Therapy for Acute Stroke : a Supplement to the Guidelines for the Management of Patients with Acute Ischemic Stroke. A statement for healthcare professionals from a Special Writing Group of the Stroke Council, American Heart Association. Stroke 27 : 1711—1718, 1996
2) The National Institute of Neurological Disorders and Stroke rt-PA Stroke Study Group : Tissue plasminogen activator for acute ischemic stroke. N Engl J Med 333 : 1581—1587, 1995
3) Furlan A, Higashida R, Wechsler L, et al : Intra-arterial prourokinase for acute ischemic stroke. The PROACT II study : a randomized controlled trial. Prolyse in Acute Cerebral Thromboembolism. JAMA 282 : 2003—2011, 1999
4) 森　悦朗：血栓溶解療法の現状と展望．脳神経外科　31：249—260, 2003
5) Mori E, Yoneda Y, Tabuchi M, et al : Intravenous recombinant tissue plasminogen activator in acute carotid artery territory stroke. Neurology, 42 : 976—982, 1992
6) Yamaguchi T, Hayakawa T, Kikuchi H, et al : Intravenous tissue plasminogen activator ameliorates the outcome of hyperacute embolic stroke. Cerebrovasc Dis 3 : 269—272, 1993
7) 小川　彰：MELT Japan中間報告．脳神経外科ジャーナル　12：278, 2003
8) MELT研究班：MELT Japanホームページ．http://melt.umin.ac.jp/index.htm
9) Katzan IL, Furlan AJ, Lloyd LE, et al : Use of tissue-type plasminogen activator for acute is-

chemic stroke : the Cleveland area experience. JAMA 283 : 1151—1158, 2000
10) Yoneda Y, Mori E, Uehara T, et al : Referral and care for acute ischemic stroke in a Japanese tertiary emergency hospital. Eur J Neurol 8 : 483—488, 2001
11) Hacke W, Donnan G, Fieschi C, et al : Association of outcome with early stroke treatment : pooled analysis of ATLANTIS, ECASS, and NINDS rt-PA stroke trials. Lancet 363 : 768—774, 2004
12) Heuschmann PU, Berger K, Misselwitz B, et al : Frequency of thrombolytic therapy in patients with acute ischemic stroke and the risk of in-hospital mortality : the German Stroke Registers Study Group. Stroke 34 : 1106—1113, 2003
13) Graham GD : Tissue plasminogen activator for acute ischemic stroke in clinical practice : a meta-analysis of safety data. Stroke 34 : 2847—2850, 2003

Abstract

Thrombolytic therapy for acute ischemic stroke : An update

Etsuro Mori, M.D., Ph.D.
Department of Behavioral Neurology and Cognitive Neuroscience
Tohoku University Graduate School of Medicine

Several studies have proven the usefulness of thrombolytic agents in the therapy of ischemic stroke. Thrombolysis is an approved and generally recommended treatment for acute stroke within three hours after the onset of symptoms in north America and Europe. However, it has not approved in Japan yet. This update summarizes the current status of two ongoing clinical trials of thrombolytic therapy in Japan ; (1) Japan Alteplase Clinical Trial (J-ACT), which is a prospective, open-label trial of intravenous alteplase (0.6mg/kgBW) for all types of ischemic stroke within 3 hours of onset, and (2) Middle Cerebral Artery Embolism Local Fibrinolytic Intervention Trial (MELT Japan), which is a randomized controlled trial of intra-arterial urokinase ($\leq$600,000 IU) for middle cerebral artery occlusion within 6 hours of onset. J-ACT has been completed recently, and suggested that alteplase at the dose of at 0.6mg/kg is effective for Japanese patients with ischemic stroke comparably to that at the dose of 0.9mg/kg in US and Europe. MELT Japan is now ongoing, and the available data in an interim analysis suggests that intra-arterial urokinase is promising.

(Jpn J Stroke 26 : 647—650, 2004)

Key words : ischemic stroke, thrombolytic therapy, Clinical trial